Extraction of partonic transverse momentum distributions from semi-inclusive deep inelastic scattering and Drell-Yan data

Alessandro Bacchetta,[1,2,*] Filippo Delcarro,[1,2,†] Cristian Pisano,[1,2,*] Marco Radici,[2,‡] and Andrea Signori[3,4,5,§]

[1] *Dipartimento di Fisica, Università di Pavia, via Bassi 6, I-27100 Pavia*
[2] *INFN Sezione di Pavia, via Bassi 6, I-27100 Pavia, Italy*
[3] *Theory Center, Thomas Jefferson National Accelerator Facility, 12000 Jefferson Avenue, Newport News, VA 23606, USA*
[4] *Department of Physics and Astronomy, VU University Amsterdam, De Boelelaan 1081, NL-1081 HV Amsterdam, the Netherlands*
[5] *Nikhef, Science Park 105, NL-1098 XG Amsterdam, the Netherlands*

(Dated: Saturday 11th February, 2017, 13:19)

We present an extraction of unpolarized partonic transverse momentum distributions (TMDs) from a simultaneous fit of available data measured in semi-inclusive deep inelastic scattering and in Drell-Yan processes through the production of photon and Z bosons. To connect data at different scales, we use TMD evolution at next-to-leading logarithmic accuracy. The analysis is restricted to the low-transverse-momentum region, with no matching to fixed-order calculations at high transverse momentum. We introduce specific choices to deal with TMD evolution at low scales, of the order of 1 GeV^2. This could be considered as a first attempt at a global fit of TMDs.

PACS numbers: 13.60.Le, 13.87.Fh,14.20.Dh

I. INTRODUCTION

Parton distribution functions describe the internal structure of the nucleon in terms of its elementary constituents (quarks and gluons). They cannot be easily computed from first principles, because they require the ability to carry out Quantum Chromodynamics (QCD) calculations in a nonperturbative regime. Experimental observables in any hard scattering experiment involving hadrons are related to parton distribution functions (PDFs) and fragmentation functions (FFs) , in a way that is specified by factorization theorems (see, e.g., Refs. [1, 2]). These theorems also elucidate the universality properties of PDFs and FFs (i.e., the fact that they are the same in different processes) and their evolution equations (i.e., how they get modified by the change in the hard scale of the process). Availability of measurements of different processes in different experiments makes it possible to test the reliability of factorization theorems and extract PDFs and FFs through so-called global fits. On the other side, the knowledge of PDFs and FFs allow us to make predictions for hard hadronic processes. These general statements apply equally well to standard collinear PDFs and FFs and to transverse-momentum-dependent parton distribution functions (TMD PDFs) and fragmentation functions (TMD FFs). The PDFs describe the distribution of partons when they move collinear with the parent hadron; (or: for which the light-cone minus and transverse components of the momentum are averaged) hence, PDFs are function only of the parton longitudinal momentum fraction x. TMD PDFs include also the dependence on transverse momentum components $k_\perp^2$. They can be interpreted as three-dimensional generalizations of standard PDFs. Similar arguments apply to FFs and TMD FFs.

Apart from the many similarities, there are also several differences between collinear and TMD distributions. From the formal point of view, factorization theorems for the two types of functions are qualitatively different, implying also different universality properties and evolution equations [3]. From the experimental point of view, observables related to TMDs require the measurement of some transverse momentum component much smaller than the hard scale of the process [4, 5]. For instance, Deep-Inelastic Scattering (DIS) is characterized by a hard scale represented by the 4-momentum squared of the virtual photon ($-Q^2$). In inclusive DIS this is the only scale of the process, and access is limited to collinear PDFs and FFs. In semi-inclusive DIS (SIDIS) also the transverse momentum of the outgoing detected hadron (P_{hT}) can be measured [6, 7]. If $P_{hT}^2 \ll Q^2$, TMD factorization can be applied and the process is sensitive to TMDs [2].

*Electronic address: alessandro.bacchetta@unipv.it
†Electronic address: filippo.delcarro01@ateneopv.it
‡Electronic address: marco.radici@pv.infn.it
§Electronic address: asignori@jlab.org

If polarization is taken into account, several TMDs can be introduced [6, 8, 9] and possibly extracted from measurements [10–12]. In this work, we focus on the simplest ones, i.e., the unpolarized TMD PDF $f_1^q(x, k_\perp^2)$ and the unpolarized TMD FF $D_1^{q\to h}(z, P_{hT}^2)$, where z is the fractional energy carried by the detected hadron h. Despite their simplicity, the phenomenology of these unpolarized TMDs present several challenges [13]: the functional form of TMDs at low partonic transverse momentum, its possible dependence on the parton flavor [14], the implementation of TMD evolution [3, 15], the matching to fixed-order calculations in collinear factorization [16].

We take into consideration three kinds of processes: SIDIS, and Drell–Yan processes (DY) with the production of virtual photons and Z bosons. To date, they represent almost all possible processes where experimental information is available for unpolarized TMD extractions. The only important process currently missing is electron-positron annihilation, which is particularly important for the determination of TMD FFs [15]. This work can therefore be considered as the first attempt at a global fit of TMDs.

The paper is organized as follows. In Sec. II, the general formalism for TMDs in SIDIS and DY processes is briefly outlined, including a description of the assumptions and approximations in the phenomenological implementation of TMD evolution equations. In Sec. **??**, the criteria for selecting the data analyzed in the fit are summarized and commented. In Sec. IV, the results of our global fit are presented and discussed. In Sec. V, we draw some conclusions.

II. FORMALISM

Shall we add pictures for the kinematics of SIDIS and DY data ? E.g. see Fig. 1 in [14].

A. Semi-inclusive DIS

In one-particle SIDIS, a lepton ℓ with momentum l scatters off a hadron target N with mass M and momentum P. In the final state, the scattered lepton momentum l' is measured together with one hadron h with mass M_h and momentum P_h. The corresponding reaction formula is

$$\ell(l) + N(P) \to \ell(l') + h(P_h) + X\,. \tag{1}$$

The space-like momentum transfer is $q = l - l'$, with $Q^2 = -q^2$. We introduce the usual invariants

$$x = \frac{Q^2}{2\,P\cdot q}, \qquad y = \frac{P\cdot q}{P\cdot l}, \qquad z = \frac{P\cdot P_h}{P\cdot q}, \qquad \gamma = \frac{2Mx}{Q}. \tag{2}$$

The available data refer to SIDIS hadron multiplicities, namely to the differential number of hadrons produced per corresponding inclusive DIS event. In terms of cross sections, we define the multiplicities as

$$m_N^h(x, z, |\boldsymbol{P}_{hT}|, Q^2) = \frac{d\sigma_N^h/(dxdzd|\boldsymbol{P}_{hT}|dQ^2)}{d\sigma_{\rm DIS}/(dxdQ^2)}\,, \tag{3}$$

where $d\sigma_N^h$ is the differential cross section for the SIDIS process and $d\sigma_{\rm DIS}$ is the corresponding inclusive one, and where $\boldsymbol{P}_{hT}$ is the component of $\boldsymbol{P}_h$ transverse to $\boldsymbol{q}$. In the single-photon-exchange approximation, the multiplicities can be written as ratios of structure functions (see [7] for details):

$$m_N^h(x, z, |\boldsymbol{P}_{hT}|, Q^2) = \frac{2\pi\,|\boldsymbol{P}_{hT}|F_{UU,T}(x, z, \boldsymbol{P}_{hT}^2, Q^2) + 2\pi\varepsilon|\boldsymbol{P}_{hT}|F_{UU,L}(x, z, \boldsymbol{P}_{hT}^2, Q^2)}{F_T(x, Q^2) + \varepsilon F_L(x, Q^2)}\,, \tag{4}$$

where

$$\varepsilon = \frac{1 - y - \frac{1}{4}\gamma^2 y^2}{1 - y + \frac{1}{2}y^2 + \frac{1}{4}\gamma^2 y^2}\,, \tag{5}$$

and the structure function $F_{XY,Z}$ corresponds to a lepton with polarization X scattering on a target with polarization Y by exchanging a virtual photon in a polarization state Z.

The semi-inclusive cross section can be expressed in a factorized form in terms of TMDs only in the kinematical limits $M^2 \ll Q^2$ and $\boldsymbol{P}_T^2 \ll Q^2$. In these limits, the structure function $F_{UU,L}$ of Eq. (4) can be neglected [17]. The structure function F_L in the denominator contains contributions involving powers of the strong coupling constant

α_S at an order that goes beyond the level reached in this analysis; hence, it will be consistently neglected (see also Ref. [14]).

To express the structure functions in terms of TMD distribution and fragmentation functions, we rely on the factorized formula for SIDIS at low transverse momenta [2, 18–25]:

$$\begin{aligned} F_{UU,T}(x,z,\boldsymbol{P}_{hT}^2,Q^2) &= \sum_a \mathcal{H}^a_{UU,T}(Q^2;\mu^2) \\ &\times \int d\boldsymbol{k}_\perp\, d\boldsymbol{P}_\perp\, f_1^a\big(x,\boldsymbol{k}_\perp^2;\mu^2\big)\, D_1^{a\to h}\big(z,\boldsymbol{P}_\perp^2;\mu^2\big)\, \delta\big(z\boldsymbol{k}_\perp - \boldsymbol{P}_{hT} + \boldsymbol{P}_\perp\big) \\ &+ Y_{UU,T}\big(Q^2,\boldsymbol{P}_{hT}^2\big) + \mathcal{O}\big(M^2/Q^2\big)\,. \end{aligned} \tag{6}$$

Here, $\mathcal{H}_{UU,T}$ is the hard scattering part; $f_1^a(x,\boldsymbol{k}_\perp^2;\mu^2)$ is the TMD distribution of unpolarized partons with flavor a in an unpolarized proton, carrying longitudinal momentum fraction x and transverse momentum $\boldsymbol{k}_\perp$ at the factorization scale μ^2, which in the following we choose to be equal to Q^2. The $D_1^{a\to h}(z,\boldsymbol{P}_\perp^2;\mu^2)$ is the function describing the fragmentation of an unpolarized parton with flavor a into an unpolarized hadron h carrying longitudinal momentum fraction z and transverse momentum $\boldsymbol{P}_\perp$. The term $Y_{UU,T}$ is introduced to ensure a matching to the perturbative fixed-order calculations at higher transverse momenta.

Specific challenges related to the application of the TMD formalism to SIDIS at low Q have been recently pointed out [16]. In our work, we leave a detailed treatment of the matching to the high $P_{hT} \approx Q$ region to future investigations. Here, because of the above kinematical limits the $Y_{UU,T}$ term and corrections from higher twists of order M^2/Q^2 or higher can be neglected. Moreover, in this analysis we resum the soft gluon radiation up to the Next-to-Leading-Log level (NLL). Consistently, the hard scattering part is computed at leading order in α_S, namely $\mathcal{H}_{UU,T}(Q^2,\mu^2) \approx 1$.

To the purpose of applying TMD evolution equations, we need to calculate the Fourier transform of the the part of Eq. (6) involving TMDs. The structure function thus reduces to

$$F_{UU,T}(x,z,\boldsymbol{P}_{hT}^2,Q^2) \approx \sum_a \int_0^\infty \frac{db_T}{2\pi} b_T J_0\big(b_T|\boldsymbol{P}_{hT}|/z\big) \tilde{f}_1^a\big(x,b_T;\mu^2\big) \tilde{D}_1^{a\to h}\big(z,b_T;\mu^2\big)\,.$$

E' questa la formula usata nel codice, o serve dire altro?

B. Drell–Yan processes

In a Drell–Yan process, two hadrons A and B with momenta P_A and P_B collide at a center-of-mass energy squared $s = (P_A + P_B)^2$ and produce a virtual photon or a Z boson plus hadrons. The boson decays into a lepton-antilepton pair. The reaction formula is

$$A(P_A) + B(P_B) \to [\gamma^*/Z + X \to] \ell^+(l) + \ell^-(l') + X. \tag{7}$$

The invariant mass of the virtual photon is $Q^2 = q^2$ with $q = l + l'$. We introduce the rapidity of the virtual photon

$$\eta = \frac{1}{2}\log\left(\frac{E+q_z}{E-q_z}\right)\,. \tag{8}$$

Io preferisco la versione con q^0 oppure ν al posto di E, che potrebbe venir confusa con l'energia dello stato adronico iniziale, cioè $E = P^0$.. The cross section can be written in terms of structure functions [26, 27]. For our purposes, we need the unpolarized cross section integrated over $d\Omega$ and over the azimuthal angle of the virtual photon,

$$\frac{d\sigma}{dQ^2\, dq_T^2\, d\eta} = \sigma_0^{\gamma,Z}\left(F_{UU}^1 + \frac{1}{2}F_{UU}^2\right). \tag{9}$$

The elementary cross sections are

$$\sigma_0^\gamma = \frac{4\pi\alpha_{\rm em}^2}{3Q^2 s}, \qquad \sigma_0^Z = \frac{\pi^2\alpha_{\rm em}}{s(\sin^2\theta_W\cos^2\theta_W} B_R(Z\to\ell^+\ell^-)\delta(Q^2 - M_Z^2), \tag{10}$$

where θ_W is Weinberg's angle, M_Z is the mass of the Z boson , and B_R is the branching ratio for the Z boson decay in two leptons. We adopted the narrow-width approximation (che cosa vuol dire?). We used the values $\sin^2\theta_W = 0.2313$, $M_Z = 91.18$ GeV , and $B_R(Z\to\ell^+\ell^-) = 3.366$.

[Secondo me nella prima delle eq.(10) ci vuole π^2. Infatti, partendo da Ref.[14] abbiamo

$$\frac{d\sigma}{d^4q} = \frac{\alpha^2}{sQ^2}\,\frac{8\pi}{3}\,\left[F_{UU}^1 + \frac{1}{2}\,F_{UU}^2\right]$$

Ora $d^4q = dq^+dq^-dq_xdq_y$. Lo Jacobiano della trasformazione $||dQ^2d\eta/dq^+dq^-|| = 2$. Mentre quello per $||dq_T^2d\theta_q/dq_xdq_y|| = 2$. Quindi

$$\frac{d\sigma}{dQ^2d\eta dq_T^2d\theta_q} = \frac{1}{4}\,\frac{d\sigma}{d^4q} = \frac{\alpha^2}{sQ^2}\,\frac{2\pi}{3}\,\left[F_{UU}^1 + \frac{1}{2}\,F_{UU}^2\right]$$

L'ulteriore integrazione in $d\theta_q$ fornisce un 2π, quindi

$$\frac{d\sigma}{dQ^2d\eta dq_T^2} = \frac{\alpha^2}{sQ^2}\,\frac{4\pi^2}{3}\,\left[F_{UU}^1 + \frac{1}{2}\,F_{UU}^2\right]$$

Vi torna?]

Similarly to the SIDIS case, in the kinematical limit $q_T^2 \ll Q^2$ and neglecting the hadron masses the structure function F_{UU}^2 can be neglected.

The longitudinal momentum fractions can be written in terms of rapidity in the following way

$$x_A = \frac{Q}{\sqrt{s}}e^{\eta}, \qquad\qquad x_B = \frac{Q}{\sqrt{s}}e^{-\eta}. \tag{11}$$

[ho cambiato y in η per consistenza] Some experiments use the variable x_F, which is connected to the other variables by the following relations

$$\eta = \sinh^{-1}\left(\frac{\sqrt{s}}{Q}\frac{x_F}{2}\right), \qquad x_A = \sqrt{\frac{Q^2}{s} + \frac{x_F^2}{4}} + \frac{x_F}{2}, \qquad x_B = x_A - x_F. \tag{12}$$

The structure function F_{UU}^1 can be written as

$$\begin{aligned} F_{UU}^1(x_A, x_B, \boldsymbol{q}_T^2, Q^2) = &\sum_a \mathcal{H}_{UU}^{1a}(Q^2;\mu^2) \\ &\times \int d\boldsymbol{k}_{\perp A}\, d\boldsymbol{k}_{\perp B}\, f_1^a\big(x_A, \boldsymbol{k}_{\perp A}^2;\mu^2\big)\, f_1^{\bar a}\big(x_B, \boldsymbol{k}_{\perp B}^2;\mu^2\big)\, \delta\big(\boldsymbol{k}_{\perp A} - \boldsymbol{q}_T + \boldsymbol{k}_{\perp B}\big) \\ &+ Y_{UU}^1\big(Q^2, \boldsymbol{q}_T^2\big) + \mathcal{O}\big(M^2/Q^2\big)\,. \end{aligned} \tag{13}$$

[ho cambiato $\boldsymbol{q}_\perp$ in $\boldsymbol{q}_T$ per consistenza]

As in the SIDIS case, with the above kinematical limits the Y_{UU} term and corrections from higher twists of order M^2/Q^2 or higher can be neglected. Consistently with our NLL analysis, the hard coefficients become

$$\mathcal{H}_{UU,\gamma}^{1a}(Q^2;\mu^2) \approx \frac{e_a^2}{N_c}, \qquad\qquad \mathcal{H}_{UU,Z}^{1a}(Q^2;\mu^2) \approx \frac{V_a^2 + A_a^2}{N_c}\,, \tag{14}$$

where[1]

$$V_a = I_{3a} - 2e_a \sin\theta_W\,, \qquad\qquad A_a = I_{3a}\,. \tag{15}$$

The structure function can be conveniently expressed as a Fourier transform of the right-handside of Eq. (13) as

$$F_{UU}^1(x_A, x_B, \boldsymbol{q}_T^2, Q^2) = \sum_a \mathcal{H}_{UU}^{1a} \int_0^\infty \frac{db_T}{2\pi} b_T\, J_0\big(b_T|\boldsymbol{q}_T|\big)\, \tilde f_1^a\big(x_A, b_T;\mu^2\big)\, \tilde f_1^{\bar a}\big(x_B, b_T;\mu^2\big)\,. \tag{16}$$

Stessa osservazione che in SIDIS: è questa la formula usata nel codice, o serve dire altro?

---

[1] We remind the reader that the value of weak isospin I_3 is equal to $+1$ for u, c, t and -1 for d, s, b.

C. TMDs and their evolution

Following the CSS formalism of Refs. [2, 22], the unpolarized TMD distribution and fragmentation functions in configuration space for a parton flavor a at a certain scale μ^2 can be represented as

$$\widetilde{f}_1^a(x, b_T; \mu^2) = \sum_{i=q,\bar{q},g} \left(C_{a/i} \otimes f_1^i\right)(x, \bar{b}_*; \mu_b^2)\; e^{S(\bar{b}_*;\mu_b^2,\mu^2)}\; e^{g_K(b_T)\ln(\mu^2/Q_0^2)}\; \widetilde{f}_{1\mathrm{NP}}^a(x, b_T)\;, \tag{17}$$

$$\widetilde{D}_1^{a\to h}(z, b_T; \mu^2) = \sum_{i=q,\bar{q},g} \left(\hat{C}_{a/i} \otimes D_1^{i\to h}\right)(z, \bar{b}_*; \mu_b^2)\; e^{\hat{S}(\bar{b}_*;\mu_b^2,\mu^2)}\; e^{g_K(b_T)\ln(\mu^2/Q_0^2)}\; \widetilde{D}_{1\mathrm{NP}}^{a\to h}(z, b_T)\;. \tag{18}$$

The C and $\hat{C}$ are perturbatively calculable Wilson coefficients for the TMD distribution and fragmentation functions, respectively. They are convoluted with the corresponding collinear functions as

$$\left(C_{a/i} \otimes f_1^i\right)(x, \bar{b}_*; \mu_b^2) = \int_x^1 \frac{du}{u}\; C_{a/i}\left(\frac{x}{u}, \bar{b}_*; \mu_b^2\right)\; f_1^i(u; \mu_b^2)\;, \tag{19}$$

$$\left(\hat{C}_{a/i} \otimes D_1^{i\to h}\right)(z, \bar{b}_*; \mu_b^2) = \int_z^1 \frac{du}{u}\; \hat{C}_{a/i}\left(\frac{z}{u}, \bar{b}_*; \mu_b^2\right)\; D_1^{i\to h}(u; \mu_b^2)\;. \tag{20}$$

The convolutions are only valid for small $b_T \ll 1/\Lambda_{\mathrm{QCD}}$. At larger b_T, the TMDs need to match the nonperturbative expressions $\widetilde{f}_{1\mathrm{NP}}^a$ and $\widetilde{D}_{1\mathrm{NP}}^{a\to h}$, respectively, that must be constrained by fitting experimental data. The evolution of TMDs from the initial scale Q_0 to μ is carried out through perturbatively calculable Sudakov factors S and $\hat{S}$, respectively, and through a nonperturbative universal term g_K at large b_T that accounts for the radiation of soft gluons emitted by the considered parton.

The matching between small (perturbative) and large (nonperturbative) b_T is controlled by the μ_b scale, which naturally should be proportional to $1/b_T$. We choose

$$\mu_b = \frac{2e^{-\gamma_E}}{\bar{b}_*}\;, \tag{21}$$

where γ_E is the Euler constant and

$$\bar{b}_* \equiv b_{\max}\left(\frac{1 - e^{-b_T^4/b_{\max}^4}}{1 - e^{-b_T^4/b_{\min}^4}}\right)^{1/4}. \tag{22}$$

This variable replaces the simple dependence upon b_T in the convolutions of Eqs. (19), (20) and in the perturbative Sudakov factors S and $\hat{S}$; namely, in the perturbative parts of the TMD definitions of Eqs. (17), (18). In fact, at large b_T these parts are no longer reliable. Therefore, the $\bar{b}_*$ is chosen to saturate on the maximum value $b_{\max}$, as suggested by the CSS formalism [2, 22]. [2] On the other hand, at small b_T the TMD formalism must match the fixed-order collinear calculations where the b_T dependence is perturbatively generated. The form of the matching is arbitrary. Here, we choose to saturate $\bar{b}_*$ on the minimum value $b_{\min} \propto 1/Q$. In general, both $b_{\max}$ and $b_{\min}$ must not be considered as free parameters; rather, they should be regarded as arbitrary scales separating perturbative from nonperturbative regimes [29]. We choose to fix them on the values

$$b_{\max} = 2e^{-\gamma_E}\ \mathrm{GeV}^{-1} = 1.123\ \mathrm{GeV}^{-1}, \qquad b_{\min} = 2e^{-\gamma_E}/Q\;. \tag{23}$$

The motivations are the following:

- because of the choices (23), the scale μ_b is constrained between 1 GeV and Q, so that the collinear PDFs are never computed at a scale lower than 1 GeV and the lower limit of the integrals contained in the definition of the perturbative Sudakov factor can never become larger than the upper limit
- at $Q_0 = 1$ GeV, $b_{\max} = b_{\min}$ and there are no evolution effects; the TMD is simply given by the corresponding collinear function multiplied by a nonperturbative contribution depending on the intrinsic b_T (plus possible corrections of order α_S from the Wilson coefficients)

[2] We remind that different schemes are possible to deal with the high-b_T region like the so-called "complex-b prescription" [28].

- Our choice partially corresponds to modifying the resummed leading logarithms in the gluon radiation as in Ref. [30].

By integrating over the impact parameter b_T, the collinear expression for both distribution and fragmentation functions can be recovered.

Following Refs. [31–33], for the nonperturbative Sudakov factor we make the traditional choice $g_K(b_T) = -g_2 b_T^2/2$ with g_2 a free parameter. Recently, several alternative forms have been proposed [29, 34] including the suggestion of not including such term [35].

The intrinsic nonperturbative parts of the TMDs are

$$\widetilde{f}^{a}_{1\mathrm{NP}}(x, b_T) = e^{-\langle \boldsymbol{k}^2_{\perp a}\rangle \frac{b_T^2}{4}} \left(1 - \frac{\lambda}{1+\lambda}\, \langle \boldsymbol{k}^2_{\perp a}\rangle \frac{b_T^2}{4}\right), \tag{24}$$

$$\widetilde{D}^{a\to h}_{1\mathrm{NP}}(z, b_T) = \frac{\langle \boldsymbol{P}^2_{\perp a\to h}\rangle\, e^{-\langle \boldsymbol{P}^2_{\perp a\to h}\rangle \frac{b_T^2}{4}} + \lambda_F\, \langle \boldsymbol{P}'^2_{\perp a\to h}\rangle \left(1 - \langle \boldsymbol{P}'^2_{\perp a\to h}\rangle \frac{b_T^2}{4}\right)\, e^{-\langle \boldsymbol{P}'^2_{\perp a\to h}\rangle \frac{b_T^2}{4}}}{\langle \boldsymbol{P}^2_{\perp a\to h}\rangle + \lambda_F\, \langle \boldsymbol{P}'^2_{\perp a\to h}\rangle}\,. \tag{25}$$

After performing the anti-Fourier transform, the $f_{1\mathrm{NP}}$ and $D_{1\mathrm{NP}}$ in momentum space look like the normalized linear combination of two different Gaussians:

$$f^{a}_{1\mathrm{NP}}(x, \boldsymbol{k}_\perp) = \frac{1}{\pi}\, \frac{(1 + \lambda \boldsymbol{k}^2_\perp)}{\langle \boldsymbol{k}^2_{\perp a}\rangle + \lambda\, \langle \boldsymbol{k}^2_{\perp a}\rangle^2}\, e^{-\frac{\boldsymbol{k}^2_\perp}{\langle \boldsymbol{k}^2_{\perp a}\rangle}}\,, \tag{26}$$

$$D^{a\to h}_{1\mathrm{NP}}(z, \boldsymbol{P}_\perp) = \frac{1}{\pi}\, \frac{1}{\langle \boldsymbol{P}^2_{\perp a\to h}\rangle + \lambda_F\, \langle \boldsymbol{P}'^2_{\perp a\to h}\rangle^2} \left(e^{-\frac{\boldsymbol{P}^2_\perp}{\langle \boldsymbol{P}^2_{\perp a\to h}\rangle}} + \lambda_F\, \boldsymbol{P}^2_\perp\, e^{-\frac{\boldsymbol{P}^2_\perp}{\langle \boldsymbol{P}'^2_{\perp a\to h}\rangle}}\right). \tag{27}$$

Based on the analyses of Refs. [14, 15], the Gaussian width of the TMD distribution depends on the parton flavor a and on its fractional momentum x according to

$$\langle \boldsymbol{k}^2_{\perp a}\rangle(x) = \langle \hat{\boldsymbol{k}}^2_{\perp a}\rangle\, \frac{(1-x)^\alpha\, x^\sigma}{(1-\hat{x})^\alpha\, \hat{x}^\sigma}\,, \tag{28}$$

where α, σ, and $\langle \hat{\boldsymbol{k}}^2_{\perp a}\rangle \equiv \langle \boldsymbol{k}^2_{\perp a}\rangle(\hat{x})$ with $\hat{x} = 0.1$, are free parameters. Similarly, we have

$$\langle \boldsymbol{P}^2_{\perp a\to h}\rangle(z) = \langle \hat{\boldsymbol{P}}^2_{\perp a\to h}\rangle\, \frac{(z^\beta + \delta)\, (1-z)^\gamma}{(\hat{z}^\beta + \delta)\, (1-\hat{z})^\gamma}\,, \tag{29}$$

where β, γ, δ, and $\langle \hat{\boldsymbol{P}}^2_{\perp a\to h}\rangle \equiv \langle \boldsymbol{P}^2_{\perp a\to h}\rangle(\hat{z})$ with $\hat{z} = 0.5$, are free parameters. For sake of simplicity, the β, γ, δ parameters are taken equal for all fragmentation channels [14, 15].

III. DATA ANALYSIS

One of the main goals of our fit is to test the universality of TMD parton distributions and fragmentation functions among different processes. To achieve this we included measurements taken from semi-inclusive DIS, Drell-Yan and Z boson production from a wide range of experimental collaborations. In this chapter we will illustrate the experimental data considered for each process and the reasons behind the kinematic cuts applied to them.

Tab. III D refers to the experimental data for SIDIS off proton target (HERMES experiment) and presents its kinematic features. The same holds for Tab. III D, Tab. III D, Tab. III D for SIDIS off deuteron (HERMES and COMPASS experiments), Drell-Yan events at low energy and Z boson production.

A. Hermes data

The semi-inclusive DIS data are taken from HERMES collaboration [36] and COMPASS experiment [37]. A similar analysis on HERMES data has been alredy done in a previous work [14].

HERMES data are grouped in two data sets, distinguished by the inclusion or subtraction of the vector meson contribution. In our work we considered only the vector meson subtracted data set.

The collaboration measured the multiplicities for SIDIS in a fixed target experiment using hydrogen and deuteron and separating charged pions and kaons produced in the final state. The data set then includes 8 different channels for every combination of target and final-state hadron for a total of 2688 points.

They are divided in bins of (x, z, Q^2, Ph_T) with the average values of (x, Q^2) spanning from about $(0.04, 1.25\ \text{GeV}^2)$ to $(0.4, 9.2\ \text{GeV}^2)$, while for other variables we have $0.1 \leq z \leq 0.9$ and $0.1\text{GeV} \leq |Ph_T| \leq 1$ GeV.

B. Compass data

Compass collaboration instead extracted multiplicities of charged hadrons produced in SIDIS on a deuteron (^{6}LiD) target. The data are organised in bins dependent on (x, z, Q^2, Ph_T) as well, however the number of data is an order of magnitude greater than the HERMES ones.

The data cover the range of (x, Q^2) from $(0.0052, 1.11\text{GeV}^2)$ to $(0.0932, 7.57\text{GeV}^2)$ and the interval $0.2 \leq z \leq 0.8$.

In data sets from both collaborations, for every bin we used the average values for each kinematic variables.

To avoid issues relative to errors in the normalization of data, we divided every Compass data point by the value of the first data point of their bin, defining a new variable:

$$m_{\text{norm}} = \frac{m_N^h(x, z, \boldsymbol{P}_{hT}^2, Q^2)}{m_N^h(x, z, \text{Min}[\boldsymbol{P}_{hT}^2], Q^2)} \tag{30}$$

The first data point of every selected bin was consequently considered as a fixed parameter and excluded from the degrees of freedom of the system.

The application of the TMD formalism to SIDIS at low energy Q crucially depends on the capability of separating the current from the target fragmentation region and from a soft region. The issue has been recently discussed in [38]. In this paper, we do not implement any combined cut on z and P_{hT}. We leave it to future studies[3]

C. Low-energy Drell-Yan data

In the case of Drell-Yan data we started our analysis on data sets considered in previous works [CITE]. We used data from E288 [39] measured at $\sqrt{s} = 19.4$, 23.8 and 27.4 Gev^2, denoted with the name 200, 300 and 400 respectively. We included also data from E605 [40] at $\sqrt{s} = 38.8$ GeV^2.

---

[3] The implementation of the R cut proposed in [38] crucially depends on the value of $\langle k_T^2 \rangle$, features that requires independent determinations of the quark properties.

D. Z-boson production data

We needed also data at higher q_T, so we considered also data taken from Z boson production in collider experiments at Tevatron. We used data from CDF and D0, from Run I [41, 42] at $\sqrt{s} = 1.8$ TeV and Run II [43, 44] at $\sqrt{s} = 1.96$ TeV. The invariant mass for this kind of experiments is $M = M_Z$, while the transverse momentum exchanged spans $0 < q_T < 20$GeV. The quantity used in the fit for Z boson production data is $d\sigma/dq_T$, however in the case of D0 Run II the data published contain the quantity $1/\sigma \times d\sigma/dq_T$ so we multiplied every one of this point for the cross section of this process $\sigma_{exp} = 255.8 \pm 16$ pb. The errors relative to the cross section and the data published have been added in quadrature.

Cuts and reasons
ERRORS

	HERMES $p \to \pi^+$	HERMES $p \to \pi^-$	HERMES $p \to K^+$	HERMES $p \to K^-$
Reference	[36]			
Cuts	$Q^2 > 1.4$ GeV^2 $0.2 < z < 0.7$ $P_{hT} < \text{Min}[0.2\ Q, 0.7\ Qz] + 0.5$ GeV			
Points	188	186	187	185
Max. Q^2	9.2 GeV^2			
x range	$0.06 < x < 0.4$			

TABLE I: Semi-inclusive DIS proton-target data (Hermes experiment).

	HERMES $D \to \pi^+$	HERMES $D \to \pi^-$	HERMES $D \to K^+$	HERMES $D \to K^-$	COMPASS $D \to h^+$	COMPASS $D \to h^-$
Reference	[36]				[37]	
Cuts	$Q^2 > 1.4$ GeV^2 $0.2 < z < 0.7$ $P_{hT} < \text{Min}[0.2\ Q, 0.7\ Qz] + 0.5$ GeV					
Points	188	188	186	187	3024	3021
Max. Q^2	9.2 GeV^2				10 GeV^2	
x range	$0.06 < x < 0.4$				$0.006 < x < 0.12$	
Notes					Observable: $\frac{m_N^h(x,z,\boldsymbol{P}_{hT}^2,Q^2)}{m_N^h(x,z,\text{Min}[\boldsymbol{P}_{hT}^2],Q^2)}$	

TABLE II: Semi-inclusive DIS deuteron-target data (Hermes and Compass experiments).

E. The replica method

Description of the replica method and the definition of the χ^2 (error function).
The following text is copy-pasted from [14]. We need to edit/rewrite it. Explain: which sources of theoretical errors are we considering in the current fit, apart from the error on the collinear fragmentation functions?
The fit and the error analysis were carried out using a similar Monte Carlo approach as in Ref. [45], and taking inspiration from the work of the NNPDF collaboration (see, e.g., [46–48]). The approach consists in creating $\mathcal{M}$ replicas of the data points. In each replica (denoted by the index r), each data point i is shifted by a Gaussian noise with the same variance as the measurement. Each replica, therefore, represents a possible outcome of an independent experimental measurement, which we denote by $m_{N,r}^h(x,z,\boldsymbol{P}_{hT}^2,Q^2)$. The number of replicas is chosen so that the

	E288 200	E288 300	E288 400	E605
Reference	[39]	[39]	[39]	[40]
Cuts	$q_T < 0.2\ Q + 0.5$ GeV			
Points	45	45	78	35
$\sqrt{s}$	19.4 GeV	23.8 GeV	27.4 GeV	38.8 GeV
Q range	4-9 GeV	4-9 GeV	5-9, 11-14 GeV	7-9, 10.5-18 GeV
Kin. var.	y=0.4	y=0.21	y=0.03	$-0.1 < x_F < 0.2$

TABLE III: Low energy Drell-Yan data collected by the E288 and E605 experiments at Tevatron, with different center-of-mass energies.

	CDF Run I	D0 Run I	CDF Run II	D0 Run II
Reference	[41]	[42]	[43]	[44]
Cuts	$q_T < 0.2\ Q + 0.5$ GeV $= 18.7$ GeV			
Points	31	14	37	8
$\sqrt{s}$	1.8 TeV	1.8 TeV	1.96 TeV	1.96 TeV
Normalization	1.114	0.992	1.049	1.048

TABLE IV: Z boson production data collected by the CDF and D0 experiments at Tevatron, with different center-of-mass energies. Discuss the meaning of the normalization factors.

mean and standard deviation of the set of replicas accurately reproduces the original data points. In our case, we have found that 200 replicas are more than sufficient.

The standard minimization procedure is applied to each replica separately, by minimizing the following error function [4]

$$E_r^2(\{p\}) = \sum_i \frac{\left(m^h_{N,r}(x_i, z_i, \boldsymbol{P}^2_{hTi}, Q^2_i) - m^h_{N,\text{theo}}(x_i, z_i, \boldsymbol{P}^2_{hTi}; \{p\})\right)^2}{\left(\Delta m^{h\,2}_{N,\text{stat}} + \Delta m^{h\,2}_{N,\text{sys}}\right)(x_i, z_i, \boldsymbol{P}^2_{hTi}, Q^2_i) + \left(\Delta m^h_{N,\text{theo}}(x_i, z_i, \boldsymbol{P}^2_{hTi})\right)^2}. \tag{31}$$

The sum runs over the i experimental points, including all species of targets N and final-state hadrons h. The theoretical multiplicities $m^h_{N,\text{theo}}$ and their error $\Delta m^h_{N,\text{theo}}$ do not depend on Q^2, as explained in the previous section. They are computed at the fixed value $Q^2 = 2.4$ GeV^2 using the formula in Eq. (**??**). However, in each z bin for each replica the value of $D_1^{a\to h}$ is independently modified with a Gaussian noise with standard deviation equal to the theoretical error $\Delta D_1^{a\to h}$. The latter is estimated from the plots in Ref. [49] and it represents the main source of uncertainty in $\Delta m^h_{N,\text{theo}}$. Finally, the symbol $\{p\}$ denotes the vector of fitting parameters.

The minimization was carried out using the MINUIT code. The final outcome is a set of $\mathcal{M}$ different vectors of best-fit parameters, $\{p_{0r}\}$, $r = 1, \ldots \mathcal{M}$, with which we can calculate any observable, its mean, and its standard deviation. The distribution of these values needs not to be necessarily Gaussian. In this case, the 1σ confidence interval is different from the 68% interval. The 68% confidence interval can simply be computed for each experimental point by rejecting the largest and the lowest 16% of the $\mathcal{M}$ values.

Although the minimization is performed on the function defined in Eq. (31), the agreement of the $\mathcal{M}$ replicas with the original data is better expressed in terms of a χ^2 function defined as in Eq. (31) but with the replacement $m^h_{N,r} \to m^h_N$, i.e., with respect to the original data set. If the model is able to give a good description of the data, the distribution of the $\mathcal{M}$ values of χ^2/d.o.f. should be peaked around one.

[4] Note that the error for each replica is taken to be equal to the error on the original data points. This is consistent with the fact that the variance of the $\mathcal{M}$ replicas should reproduce the variance of the original data points.

IV. RESULTS

In the following we detail the results of fits to the data sets presented in Sec. III. In Sec. IV A we present a fit of TMDs with flavor-independent widths (see Eqs. (24) and (25)); in Sec. IV B we discuss the flavor-dependent case.

A. Flavor independent fit

In Tab. V we present the total χ^2 and its breakdown (division) between SIDIS (separating Hermes and Compass) and Drell-Yan/Z events. χ^2 values need to be added. Tab. VI summarizes the values of the nonperturbative parameters $b_{\rm min}$ and $b_{\rm max}$ (which delimit the range in b_T where transverse momentum resummation is computed perturbatively) and g_2, whcih quantifies the amount of soft gluons radiated. Tab. VII collects the best-fit values for the quantities used to parametrize the nonperturbative part of the TMDs (Eqs. (24) and (25)); central values and standard deviations are based on the replica methodology (see Sec. III E), using 68% confidence levels.

Points	Parameters	χ^2	χ^2/d.o.f.	Points HERMES	χ^2 HERMES	Points COMPASS	χ^2 COMPASS	Points DY & Z	χ^2 DY & Z
8156	11	12629 ± 363	1.55 ± 0.05	1737		6126		293	

TABLE V: Flavor-independent fit: number of points analyzed and χ^2 values for SIDIS and Drell-Yan/Z production.

$b_{\rm max}$ (fixed)	$b_{\rm min}$ (fixed)	g_2 [GeV^2]
$2e^{-\gamma_E}$/GeV	$2e^{-\gamma_E}/Q$	0.12 ± 0.01

TABLE VI: Flavor-independent fit: values of parameters common to TMD PDFs and TMD FFs.

TMD PDFs	$\langle \hat{\boldsymbol{k}}_\perp^2 \rangle$ [GeV^2]	α (random)	σ		λ	
	0.31 ± 0.08	2.93 ± 0.07	0.20 ± 0.01		1.49 ± 0.96	
TMD FFs	$\langle \hat{\boldsymbol{P}}_\perp^2 \rangle$ [GeV^2]	β	δ	γ	λ_F	$\langle \hat{\boldsymbol{P}}_\perp'^2 \rangle$ [GeV^2]
	0.20 ± 0.01	2.7 ± 0.1	3.4 ± 0.1	0.041 ± 0.004	4.9 ± 1.2	0.040 ± 0.001

TABLE VII: Flavor-independent fit: 68% confidence intervals of best-fit parameters for TMD PDFs and TMD FFs.

1. *Average transverse momenta*

2. *Kinematic dependence*

Average square transverse momenta and their kinematic dependence. (version from Dropbox, Feb. 9^{th}). Full sets of replicas and 68% confidence level bands compared to the results from other fits. Fix some of the labels on the vertical axis.

B. Flavor dependent fit

We'll see what we want to discuss here. In Tab. VIII Tab. IX Tab. X.
Description of Hermes data (version from Dropbox, Feb. 9^{th}). Legend for z values needs to be added too.
Description of Compass data (version from Dropbox, Feb. 9^{th}).

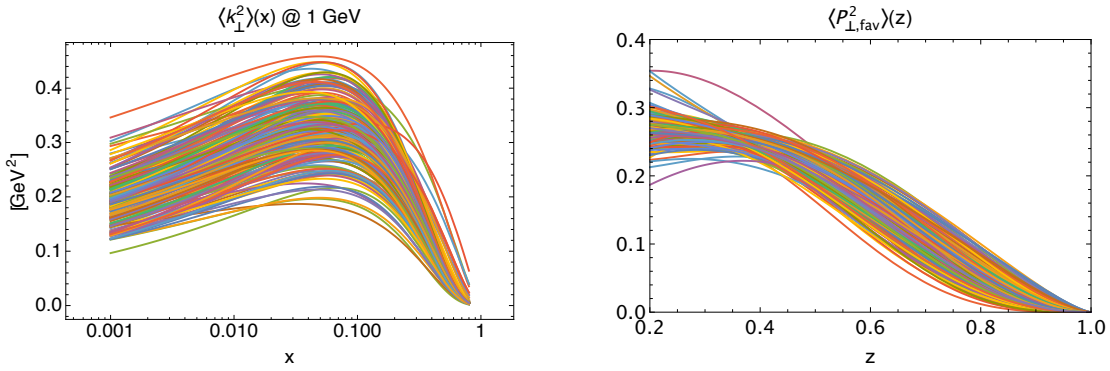

(a) (b)

FIG. 1: write the caption here (a) and another here (b).

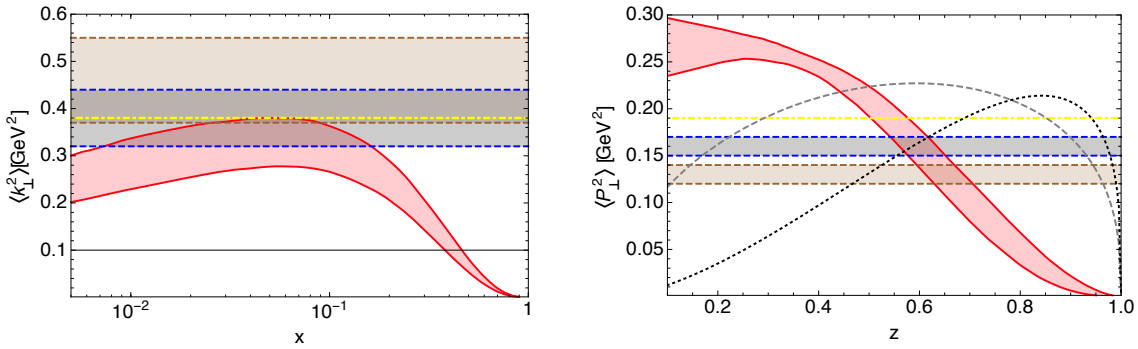

(a) (b)

FIG. 2: write the caption here (a) and another here (b).

Points	Parameters	χ^2	χ^2/d.o.f.	Points HERMES	χ^2 HERMES	Points COMPASS	χ^2 COMPASS	Points DY & Z	χ^2 DY & Z
8156	18	10456±	1.28±	1737		6126		293	

TABLE VIII: Number of points analyzed and χ^2 values for the flavor-dependent fit.

$b_{\max}$ (fixed)	$b_{\min}$ (fixed)	g_2 [GeV^2]
$2e^{-\gamma_E}$/GeV	$2e^{-\gamma_E}/Q$	0.13 ± 0.01

TABLE IX: Values of parameters common to TMD PDFs and FFs (for the flavor-dependent fit).

Description of low energy Drell-Yan data (version from Dropbox, Feb. 9^{th}). Legends need to be added too. Fix the y-axis label.

Description of Z-boson production data (version from Dropbox, Feb. 9^{th}). Legends need to be added too. Fix the y-axis label.

V. CONCLUSIONS AND OUTLOOK

TMD PDFs	$\langle \hat{\boldsymbol{k}}_\perp^2 \rangle$ [GeV^2]	α (random)	σ		λ	
up valence	0.15±	0.00±	−0.93±		50.0±	
down valence	0.31±	”	”		”	
sea	0.17±	4.56±	0.27±		0.147±	
TMD FFs	$\langle \hat{\boldsymbol{P}}_\perp^2 \rangle$ [GeV^2]	β	δ	γ	λ_F	$\langle \hat{\boldsymbol{P}}_\perp'^2 \rangle$ [GeV^2]
$u \to \pi^+$	0.22±	2.6±	2.8±	0.062±	5.9±	0.139±
$d \to \pi^+$	0.24±	”	”	”	”	”
$\bar{s} \to K^+$	0.24± (random)	”	”	”	”	”
$u \to K^+$	0.22±	”	”	”	”	”

TABLE X: 68% confidence intervals of best-fit parameters for TMD PDFs and TMD FFs in the flavor-dependent fit.

Acknowledgments

This work is supported by the European Research Council (ERC) under the European Union's Horizon 2020 research and innovation program (grant agreement No. 647981, 3DSPIN). AS acknowledges support from U.S. Department of Energy contract DE-AC05-06OR23177, under which Jefferson Science Associates, LLC, manages and operates Jefferson Lab. The work of AS has been funded partly also by the program of the Stichting voor Fundamenteel Onderzoek der Materie (FOM), which is financially supported by the Nederlandse Organisatie voor Wetenschappelijk Onderzoek (NWO).

[1] J. C. Collins, D. E. Soper, and G. Sterman, Adv. Ser. Direct. High Energy Phys. **5**, 1 (1989), hep-ph/0409313.
[2] J. Collins, *Foundations of Perturbative QCD*, Cambridge Monographs on Particle Physics, Nuclear Physics and Cosmology (Cambridge University Press, 2011), ISBN 9780521855334, URL `http://books.google.it/books?id=0xGi1KW9vykC`.
[3] T. C. Rogers, Eur. Phys. J. **A52**, 153 (2016), 1509.04766.
[4] A. Bacchetta, Eur. Phys. J. **A52**, 163 (2016).
[5] M. Radici, AIP Conf. Proc. **1735**, 020003 (2016).
[6] P. J. Mulders and R. D. Tangerman, Nucl. Phys. **B461**, 197 (1996), erratum-ibid. **B484** (1997) 538, hep-ph/9510301.
[7] A. Bacchetta, M. Diehl, K. Goeke, A. Metz, P. J. Mulders, and M. Schlegel, JHEP **02**, 093 (2007), hep-ph/0611265.
[8] A. Bacchetta and P. J. Mulders, Phys. Rev. **D62**, 114004 (2000), hep-ph/0007120.
[9] D. Boer, S. Cotogno, T. van Daal, P. J. Mulders, A. Signori, and Y.-J. Zhou, JHEP **10**, 013 (2016), 1607.01654.
[10] R. Angeles-Martinez et al., Acta Phys. Polon. **B46**, 2501 (2015), 1507.05267.
[11] E. C. Aschenauer, U. D'Alesio, and F. Murgia, Eur. Phys. J. **A52**, 156 (2016), 1512.05379.
[12] M. Boglione and A. Prokudin, Eur. Phys. J. **A52**, 154 (2016), 1511.06924.
[13] A. Signori, Ph.D. thesis, Vrije U., Amsterdam (2016), URL `http://inspirehep.net/record/1493030/files/Thesis-2016-Signori.pdf`.
[14] A. Signori, A. Bacchetta, M. Radici, and G. Schnell, JHEP **1311**, 194 (2013), 1309.3507.
[15] A. Bacchetta, M. G. Echevarria, P. J. G. Mulders, M. Radici, and A. Signori, JHEP **11**, 076 (2015), 1508.00402.
[16] J. Collins, L. Gamberg, A. Prokudin, T. C. Rogers, N. Sato, and B. Wang, Phys. Rev. **D94**, 034014 (2016), 1605.00671.
[17] A. Bacchetta, D. Boer, M. Diehl, and P. J. Mulders, JHEP **08**, 023 (2008), 0803.0227.
[18] J. C. Collins and D. E. Soper, Nucl. Phys. **B193**, 381 (1981).
[19] J. C. Collins, D. E. Soper, and G. Sterman, Nucl. Phys. **B250**, 199 (1985).
[20] X. Ji and F. Yuan, Phys. Lett. **B543**, 66 (2002), hep-ph/0206057.
[21] X. Ji, J.-P. Ma, and F. Yuan, Phys. Rev. **D71**, 034005 (2005), hep-ph/0404183.
[22] S. Aybat and T. C. Rogers, Phys. Rev. **D83**, 114042 (2011), 1101.5057.
[23] M. G. Echevarria, A. Idilbi, and I. Scimemi, JHEP **1207**, 002 (2012), 1111.4996.
[24] M. G. Echevarri, A. Idilbi, A. Schfer, and I. Scimemi, Eur.Phys.J. **C73**, 2636 (2013), 1208.1281.
[25] J. C. Collins and T. C. Rogers, Phys.Rev. **D87**, 034018 (2013), 1210.2100.
[26] D. Boer and W. Vogelsang, Phys. Rev. **D74**, 014004 (2006), hep-ph/0604177.
[27] S. Arnold, A. Metz, and M. Schlegel, Phys. Rev. **D79**, 034005 (2009), 0809.2262.
[28] E. Laenen, G. F. Sterman, and W. Vogelsang, Phys. Rev. Lett. **84**, 4296 (2000), hep-ph/0002078.
[29] J. Collins and T. Rogers, Phys. Rev. **D91**, 074020 (2015), 1412.3820.

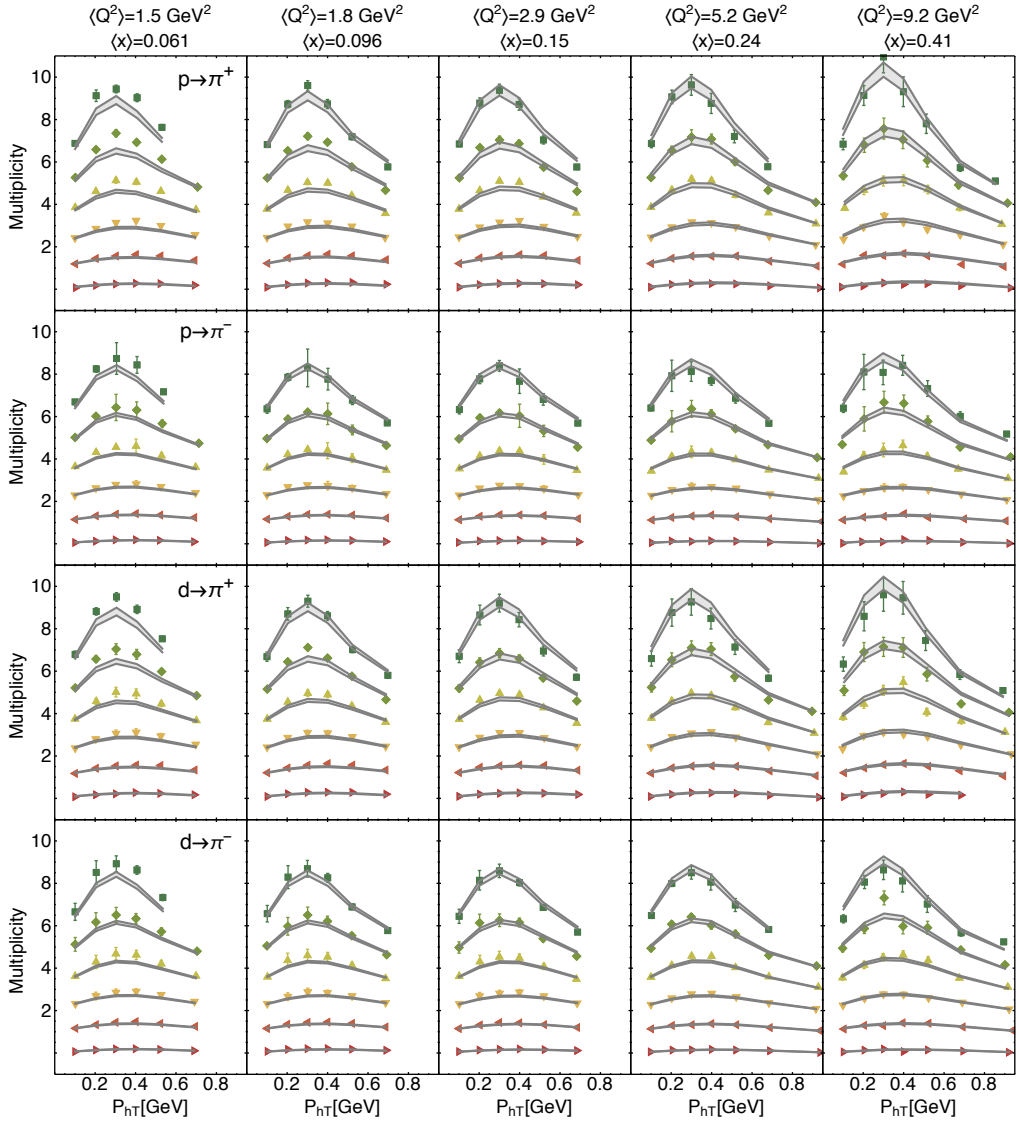

FIG. 3: Hermes multiplicities for production of pions off a proton and a deuteron for different $\langle x\rangle$, $\langle z\rangle$, and $\langle Q^2\rangle$ bins as a funciton of the transverse momentum of the dected hadron $\boldsymbol{P}_{hT}^2$.

[30] G. Bozzi, S. Catani, G. Ferrera, D. de Florian, and M. Grazzini, Phys. Lett. **B696**, 207 (2011), 1007.2351.
[31] P. M. Nadolsky, D. R. Stump, and C. P. Yuan, Phys. Rev. **D61**, 014003 (2000), hep-ph/9906280.
[32] F. Landry, R. Brock, P. M. Nadolsky, and C. P. Yuan, Phys. Rev. **D67**, 073016 (2003), hep-ph/0212159.
[33] A. V. Konychev and P. M. Nadolsky, Phys. Lett. **B633**, 710 (2006), hep-ph/0506225.
[34] C. A. Aidala, B. Field, L. P. Gamberg, and T. C. Rogers, Phys. Rev. **D89**, 094002 (2014), 1401.2654.
[35] U. D'Alesio, M. G. Echevarria, S. Melis, and I. Scimemi, JHEP **11**, 098 (2014), 1407.3311.
[36] A. Airapetian et al. (HERMES Collaboration), Phys. Rev. **D87**, 074029 (2013), 1212.5407.
[37] C. Adolph et al. (COMPASS Collaboration) (2013), 1305.7317.
[38] M. Boglione, J. Collins, L. Gamberg, J. O. Gonzalez-Hernandez, T. C. Rogers, and N. Sato, Phys. Lett. **B766**, 245 (2017), 1611.10329.
[39] A. S. Ito et al., Phys. Rev. **D23**, 604 (1981).
[40] G. Moreno et al., Phys. Rev. **D43**, 2815 (1991).
[41] T. Affolder et al. (CDF), Phys. Rev. Lett. **84**, 845 (2000), hep-ex/0001021.
[42] B. Abbott et al. (D0), Phys. Rev. **D61**, 032004 (2000), hep-ex/9907009.

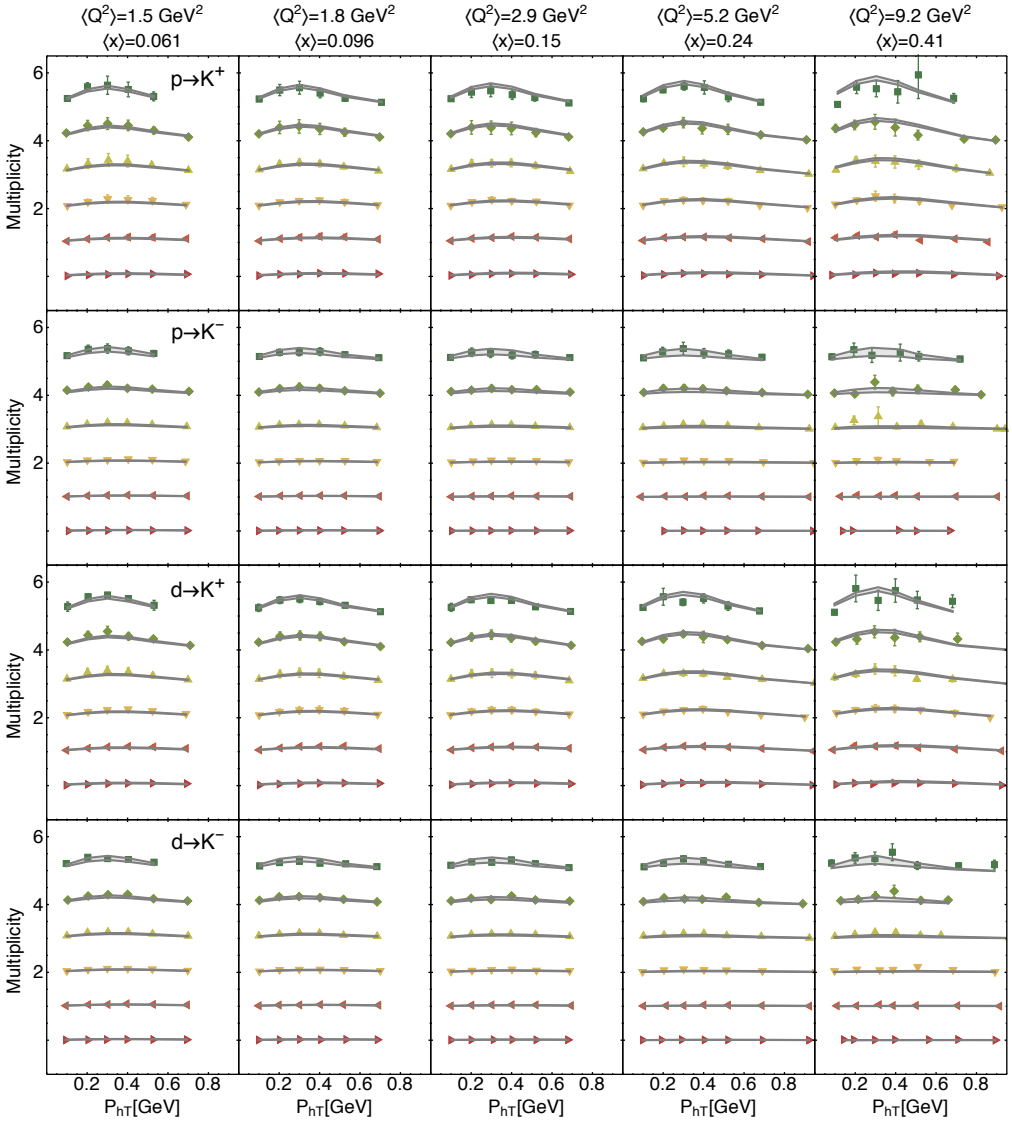

FIG. 4: Hermes multiplicities for production of kaons off a proton and a deuteron for different $\langle x\rangle$, $\langle z\rangle$, and $\langle Q^2\rangle$ bins as a funciton of the transverse momentum of the dected hadron $\boldsymbol{P}_{hT}^2$.

[43] T. Aaltonen et al. (CDF), Phys. Rev. **D86**, 052010 (2012), 1207.7138.
[44] V. M. Abazov et al. (D0), Phys. Rev. Lett. **100**, 102002 (2008), 0712.0803.
[45] A. Bacchetta, A. Courtoy, and M. Radici, JHEP **1303**, 119 (2013), 1212.3568.
[46] S. Forte, L. Garrido, J. I. Latorre, and A. Piccione, JHEP **0205**, 062 (2002), hep-ph/0204232.
[47] R. D. Ball et al. (NNPDF Collaboration), Nucl. Phys. **B809**, 1 (2009), 0808.1231.
[48] R. D. Ball et al., Nucl. Phys. **B838**, 136 (2010), 1002.4407.
[49] M. Epele, R. Llubaroff, R. Sassot, and M. Stratmann, Phys. Rev. **D86**, 074028 (2012), 1209.3240.

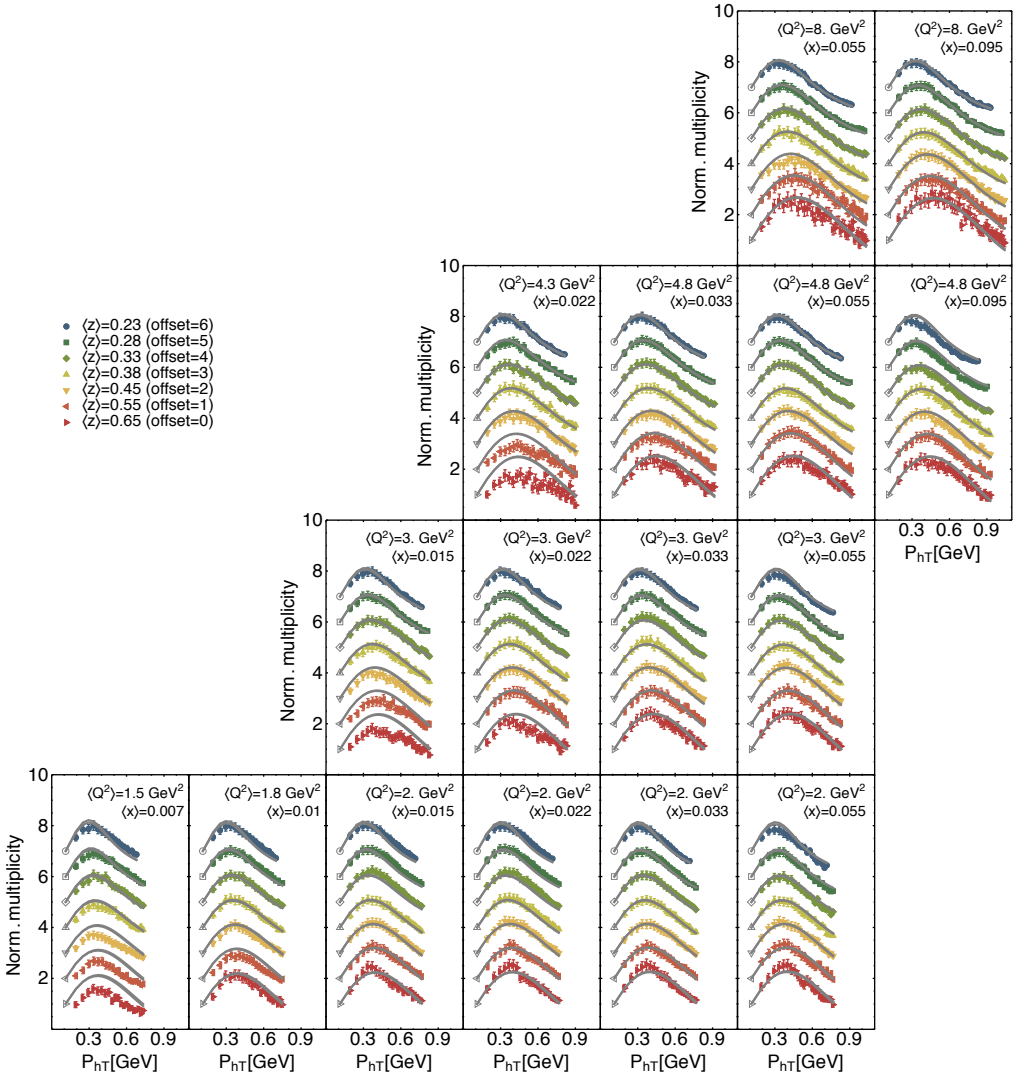

FIG. 5: Compass multiplicities for production of negative hadrons (pions) off a deuteron for different $\langle x\rangle$, $\langle z\rangle$, and $\langle Q^2\rangle$ bins as a funciton of the transverse momentum of the dected hadron $\boldsymbol{P}_{hT}^2$. Multiplicities are normalized to the first bin in $\boldsymbol{P}_{hT}^2$ for each $\langle z\rangle$ value.

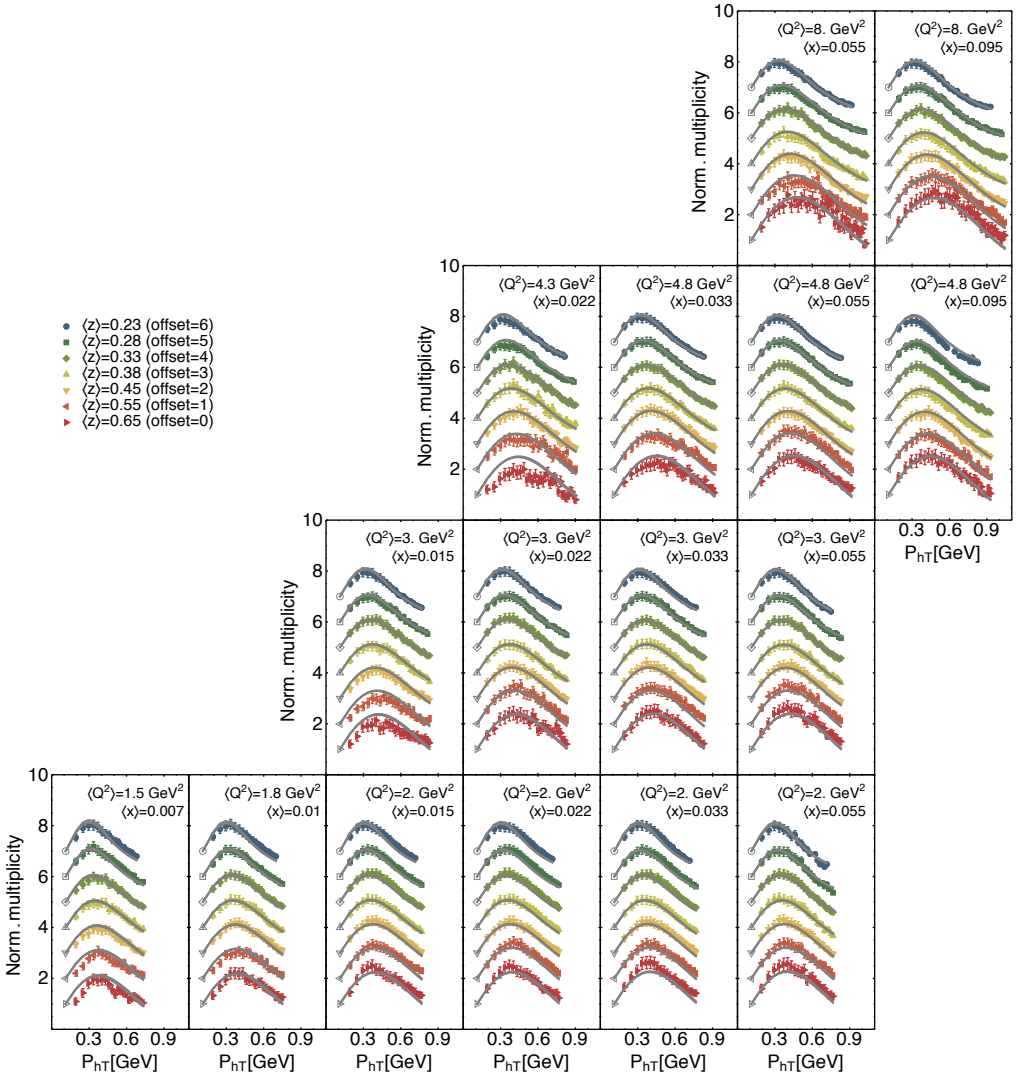

FIG. 6: Compass multiplicities for production of positive hadrons (pions) off a deuteron for different $\langle x\rangle$, $\langle z\rangle$, and $\langle Q^2\rangle$ bins as a funciton of the transverse momentum of the dected hadron $\boldsymbol{P}_{hT}^2$. Multiplicities are normalized to the first bin in $\boldsymbol{P}_{hT}^2$ for each $\langle z\rangle$ value.

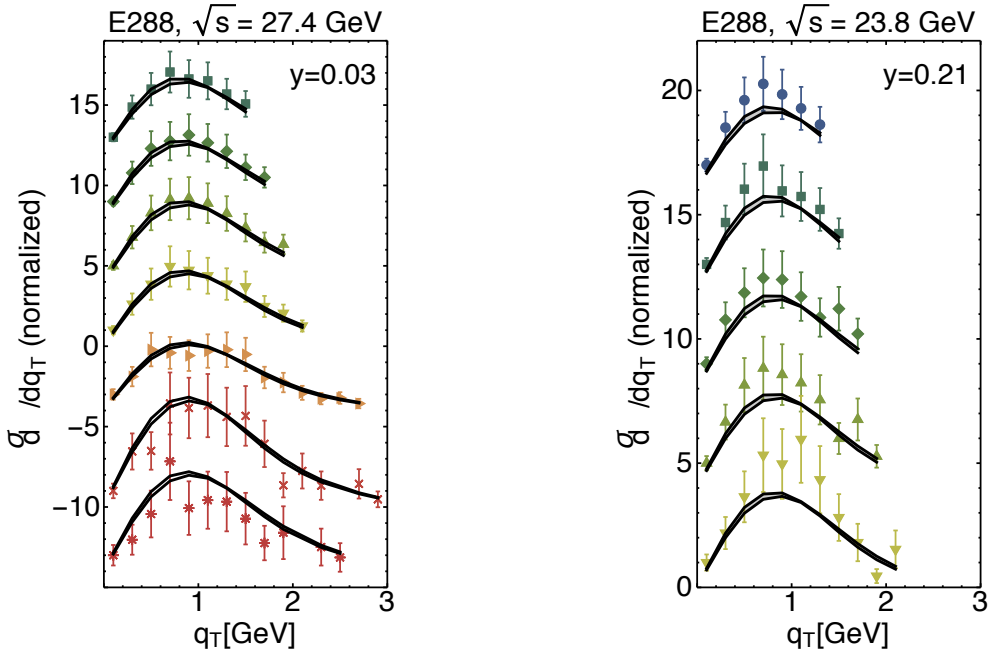

(a) (b)

FIG. 7: write the caption here (a) and another here (b).

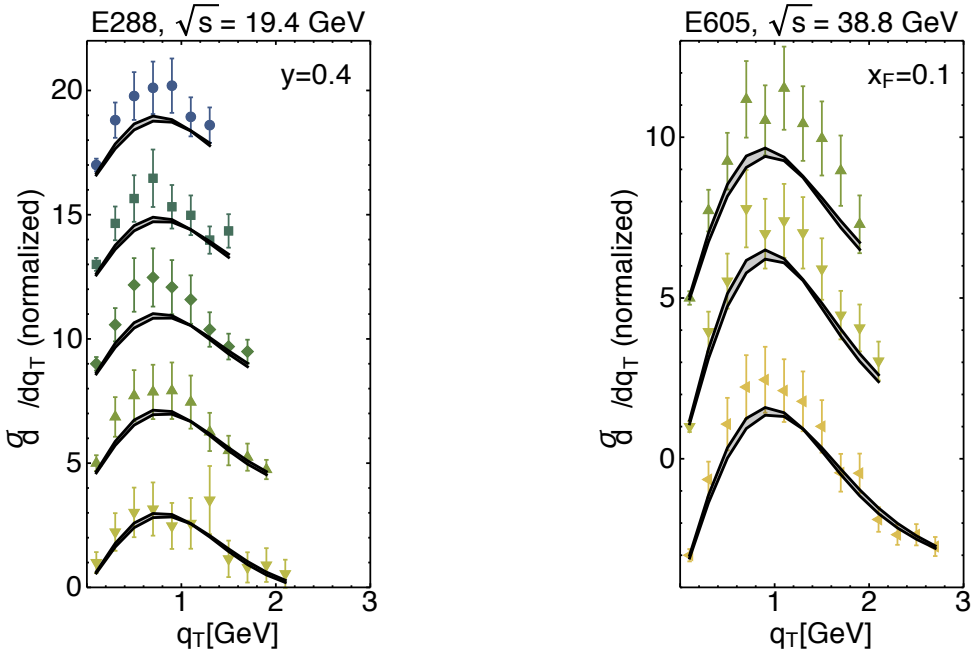

(a) (b)

FIG. 8: write the caption here (a) and another here (b).

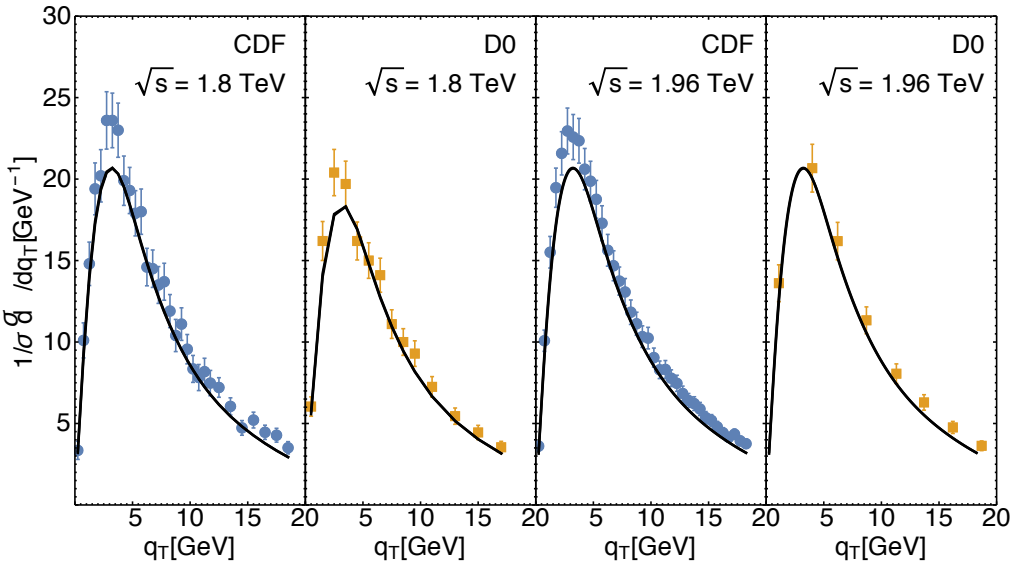

FIG. 9: Cross section differential with respect to the transverse momentum q_T of a Z boson produced from $p\bar{p}$ collisions at Tevatron. The four panels refer to different experiments (CDF and D0) with two different values for the center-of-mass energy ($\sqrt{s} = 1.96$ TeV and $\sqrt{s} = 1.8$ TeV).